# Development of a High Energy Resolution Calorimeter for the SuperNEMO Double Beta Decay Experiment

The NEMO Collaboration

**Abstract**

SuperNEMO is a double beta decay experiment, which will employ the successful tracker-calorimeter technique used in the recently completed NEMO3 [1] experiment. SuperNEMO will study 100kg of double beta decay isotope, reaching a sensitivity to a half-life greater than $10^{26}$ years for neutrinoless double beta decay ($0\nu\beta\beta$), corresponding to a Majorana neutrino mass of 50-100meV. One of the main goals and challenges of the SuperNEMO detector development programme was to reach a FWHM energy resolution of $\Delta E$/E of $\frac{7\%}{\sqrt{E(MeV)}}$ for electrons for the calorimeter, using large volume plastic scintillator blocks, which has been achieved by the collaboration.

*Keywords:* calorimeter scintillator photomultiplier

## 1. Introduction

The SuperNEMO detector [2] is based on the technology of the recently completed NEMO3 [1] experiment, using a tracker-calorimeter detection technique to study neutrinoless double beta decay ($0\nu\beta\beta$). It is the only $0\nu\beta\beta$ detector that allows full topological reconstruction of events and has the lowest projected background index as a result. The detector will hold $\sim$ 100kg of double beta decay isotope ($^{82}$Se is the 'baseline' design isotope, with $^{150}$Nd and $^{48}$Ca being considered depending on enrichment possibilities) to reach a projected sensitivity of $10^{26}$ years (50-100meV effective Majorana neutrino mass). The dominant factor in achieving the target sensitivity is the product of $\Delta$E, the energy window of the $0\nu\beta\beta$ decay at the $Q_{\beta\beta}$ value (approximated by the energy resolution of the detector in keV), and $N_{bkg}$, the expected background index in kg$^{-1}$keV$^{-1}$yr$^{-1}$: $\Delta\text{E}\times N_{bkg}$. Consequently the two main areas of focus for the SuperNEMO calorimeter R&D programme were energy resolution and radiopurity. The topology reconstruction available in SuperNEMO is a powerful tool to suppress backgrounds from natural radioactivity. However, the Standard Model of Electroweak Interaction allowed $2\nu\beta\beta$ decay will have the same topological signature as most $0\nu\beta\beta$ mechanisms. The tail of the continuum spectrum from the summed electron energy distribution of the $2\nu\beta\beta$ decay may extend into the energy window near the $Q_{\beta\beta}$ value mimicking the $0\nu\beta\beta$ process. An improved energy resolution is the only way to reduce this background and is the focus of the work described here.

The SuperNEMO detector is of a modular design (Figure 1), where the detector and the $\beta\beta$ decay source are distinct. The detector consists of 20 modules of a 4m height, 6m length and 2m width. Each module contains 5kg of a thin ($\sim$40mg/cm$^2$) vertically suspended source foil (providing a total of 100kg), surrounded by $\sim$ 2000 drift cells operating in the Geiger mode (for particle tracking) and is enclosed by calorimeter walls consisting of $\sim$520 square scintillator block and 8" photomultiplier tube

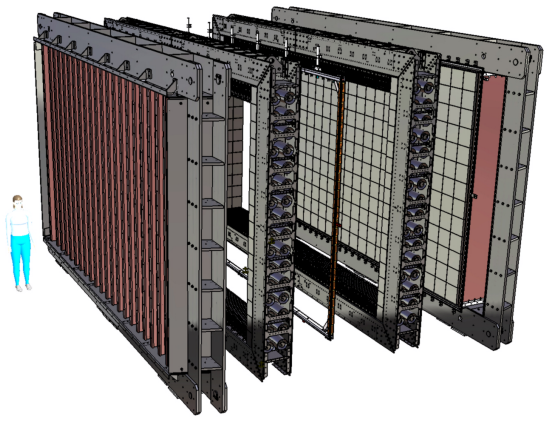

Figure 1: An exploded view of a SuperNEMO module, showing (from left to right) the calorimeter wall, tracker, source foil, tracker and calorimeter wall.

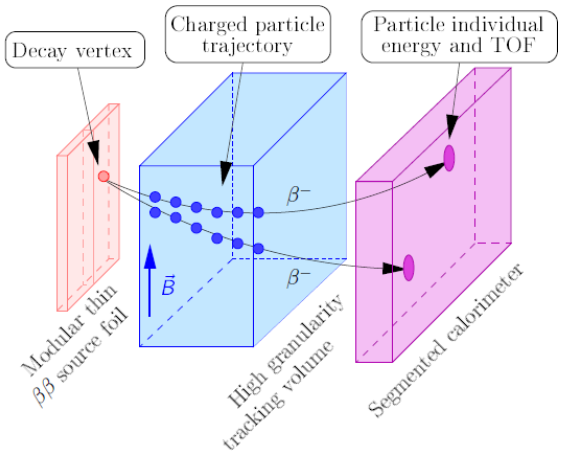


Figure 2: The SuperNEMO detector design principle.

(PMT) optical modules (for energy and time of flight measurements). The SuperNEMO detector principle is shown in Figure 2. A current carrying coil wrapped around the module produces a magnetic field of 25G to identify electrons and positrons.

The main requirements of the SuperNEMO calorimeter are to provide a good energy resolution for low energy electron ($\mathcal{O}$(1 MeV)) detection as well as efficient $\gamma$ tagging for background suppression. The SuperNEMO calorimeter must be optimised to detect incoming electrons simultaneously originating from the same vertex in the $\beta\beta$ decay source foils (Figure 2).

A calorimeter energy resolution of $\Delta E$/E of $\frac{7\%}{\sqrt{E(MeV)}}$ (or 4% FWHM at 3MeV (the $Q_{\beta\beta}$ value of $^{82}$Se)) for electrons is required to reach a sensitivy of $10^{26}$ years for SuperNEMO, as can be seen in Figure 3, which shows simulations for the SuperNEMO half-life sensitivity as a function of the calorimeter energy resolution for a fixed exposure of 500 kg.yr, where the sensitivity is a convolution of the calorimeter energy resolution and the loss of energy of the electrons exiting the source foil. When combined with other requirements, such as a good timing resolution needed to identify the simultaneous emission of two electrons of the decay and good radiopurity, developing such a detector presents a challenge. It represents a factor of two improvement from the energy resolution of the NEMO3 calorimeter, which is $\frac{14-17\%}{\sqrt{E(MeV)}}$ for electrons, for a larger volume scintillator block.

This paper will discuss the SuperNEMO calorimeter requirements (Section 2), the parameters that influence the energy resolution of a scintillator and PMT optical module (Section 3), the calorimeter test bench used to test the various parameters (Section 4), and the final SuperNEMO calorimeter design and the options tested to obtain it (Section 5).

## 2. SuperNEMO Calorimeter Requirements

SuperNEMO has a need for a robust calorimeter using reliable and time withstanding technology, with ease of manufacturing and assembly, which provides the required energy resolution at a sensible cost. The geometry and material of the scintillator blocks have to be optimised for the detection of low energy electrons whilst providing efficient $\gamma$ tagging ($>$ 50% at 1MeV) for background suppression.

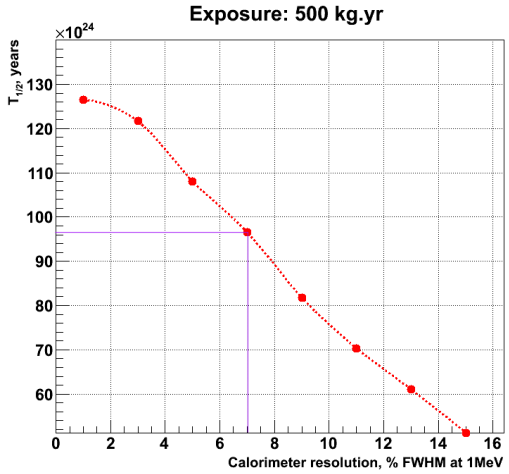


Figure 3: SuperNEMO half-life sensitivity as a function of energy resolution with a fixed exposure of 500 kg.yr for a source foil thickness of 40mg/cm$^2$ and the SuperNEMO target foil contamination of 2$\mu$Bq/kg for $^{208}$Tl, 10$\mu$Bq/kg for $^{214}$Bi and 0.15mBq/m$^3$ for $^{222}$Rn.

The calorimeter R&D for SuperNEMO consists of three main areas of study: energy resolution, radiopurity and calibration.

### *2.1. Energy Resolution*

The energy resolution of the calorimeter is required to be 7% FWHM at 1MeV for electrons to achieve the target SuperNEMO sensitivity. The scintillator geometry must be optimised to effectively fit a PMT, whilst considering the radiation detection requirements - the thickness must be at least 2cm to fully absorb the low energy electrons produced in $0\nu\beta\beta$ and >10cm for $\gamma$ interactions. A hemispherical PMT with good uniformity must be coupled to a flat face scintillator, therefore coupling options such as using a lightguide or alternatives must be considered. Good uniformity is required within a scintillator block, with the energy resolution at any point on the block not varying more than ±10% relative to the energy resolution obtained at the central position of the block. However, the block's response can also be corrected using the spatial resolution of the SuperNEMO tracking detector, which is $\sigma_{longitudinal}$ = 13mm and $\sigma_{transverse}$ = 0.7mm (measured with a 90-cell SuperNEMO tracker prototype).

The time resolution of the calorimeter is required to be 400ps $\sigma$ at 1MeV between two calorimeter counters in coincidence. This is to distinguish two electron events (the signature for $0\nu\beta\beta$) originating in the source foils and those that originate outside of the detector and then cross the active volume of the detector to immitate $0\nu\beta\beta$ events. Improving the $\Delta$E/E of the calorimeter helps to improve the time resolution. Therefore time resolution was not the focus of the R&$D$ programme but was monitored throughout.

### *2.2. Radiopurity*

Specific to low background counting experiments ultra-pure materials must be used throughout the detector. One of the main sources of contamination comes from the PMTs, specifically from the glass. The PMT radiopurity requirements depend on the double beta decay isotope being studied (the lower the $Q_{\beta\beta}$ value the more stringent the requirement) and are, depending on the level of radon emanation from the PMT glass, 100 - 500mBq/kg for $^{226}$Ra and 60 - 200mBq/kg for $^{228}$Th for the baseline design isotope. These requirements have prompted development of low-background glass on a new scale and the collaboration is currently working closely with Hamamatsu to develop a new radiopure glass to reach the radiopurity specifications of the detector.

### *2.3. Calibration*

During the five years of planned SuperNEMO data taking the gain and stability of a large number of PMTs must be monitored at a 1% level. The detector response must be linear, and any non-linear effects must be monitored at a 1% level up to 3-4MeV (the region of interest for $0\nu\beta\beta$). The absolute calibration system will use $^{207}$Bi sources (providing conversion electrons with energies of 482keV

and 976keV) inserted into the detector on a monthly basis. A daily relative calibration UV-LED based light injection system is being developed for gain and linearity monitoring. Using low activity alpha sources embedded into the scintillator to monitor the gain is an additional possibility being studied. $^{60}$Co (providing two coincident $\gamma$s of 1.1 and 1.3MeV) will occasionally be used for absolute time calibration. Calibration will not be discussed further in this paper.

## 3. Parameters Influencing Energy Resolution

Energy resolution in scintillating detectors, $\Delta$E/E, is dominated by stochastic photo-electron fluctuations. For a number of photo-electrons ($N_{pe}$) $> 20$ (as is the case for SuperNEMO), the Gaussian approximation can be used and the energy resolution can then be expressed as:

$$\frac{\Delta E}{E} = \frac{2.35\sigma}{E} = \frac{2.35}{\sqrt{N_{pe}}}. \quad (3.1)$$

The energy resolution can be shown as three experimental objectives:

$$\frac{N_{ph}}{E_e} \cdot \epsilon_{col}^{light} \cdot (QE^{PMT} \cdot \epsilon_{col}^{PMT}) = N_{pe}, \quad (3.2)$$

where $N_{ph}/E_e$ is the number of scintillation photons per unit energy and is determined by the scintillator light output. $\epsilon_{col}^{light}$ is the light collection efficiency and depends on the material, surface treatment and geometry of the scintillator, the reflector material and its efficiency and the quality of the optical coupling between the scintillator and the PMT (gels, lightguides etc). The choice of scintillator for the SuperNEMO calorimeter is discussed in Section 5.1. The critical intrinsic characteristics of the PMT include the quantum efficiency (QE) of the photocathode $QE^{PMT}$, the collection efficiency $\epsilon_{col}^{PMT}$ of photo-electrons from the photocathode to the first dynode, and the gain of the first dynode. The choice of PMT for the SuperNEMO calorimeter is discussed in Section 5.2. As can be seen in Equation 3.1, in the energy region of 1 MeV $\sim$ 1000 $N_{pe}$ are needed to achieve an $\Delta$E/E of 7%, requiring optimisation of the parameters described in Equation 3.2.

## 4. Calorimeter Test Bench

The energy resolution measurement is done on optical modules of different configurations. An optical module consists of a scintillator coupled to a PMT (either directly or using a light-guide). The measurement is carried out by exciting the scintillator with a flux of monochromatic electrons, which approximates the delta function and therefore any smearing of the distribution that is seen is due to the properties of the detector. Two electron sources are used: the main one is a $^{90}$Sr $\beta$ beam passed through a magnetic field to select monochromatic electrons of known energy, and the secondary is a $^{207}$Bi source, which provides 976keV and 482keV K-shell conversion electrons (CE). The distribution obtained with the $^{90}$Sr beam is fit with a simple Gaussian function to extract the $\Delta$E/E. The $^{207}$Bi fitting function involves the deconvolution of X-rays, $\gamma$s, L-shell and M-shell CEs coming from $^{207}$Bi to obtain the $\Delta$E/E and is used to verify the result.

Both methods have been used to study the $\Delta$E/E and have been found to be consistent. Figure 4 shows the measured energy resolution for the same optical module configuration acquired with the two different methods. The test bench measurements have been reproduced by GEANT-4 based optical MC simulations, with good agreement between the two [3] as can be seen in Figure 5, which shows a $\Delta$E/E data and MC comparison for $256^2$mm$^2$ and $308^2$mm$^2$ PST and PVT blocks.

The $^{90}$Sr variable energy beam (0.4 - 2.0 MeV) can also be used to acquire a measurement of the dependence of energy resolution on

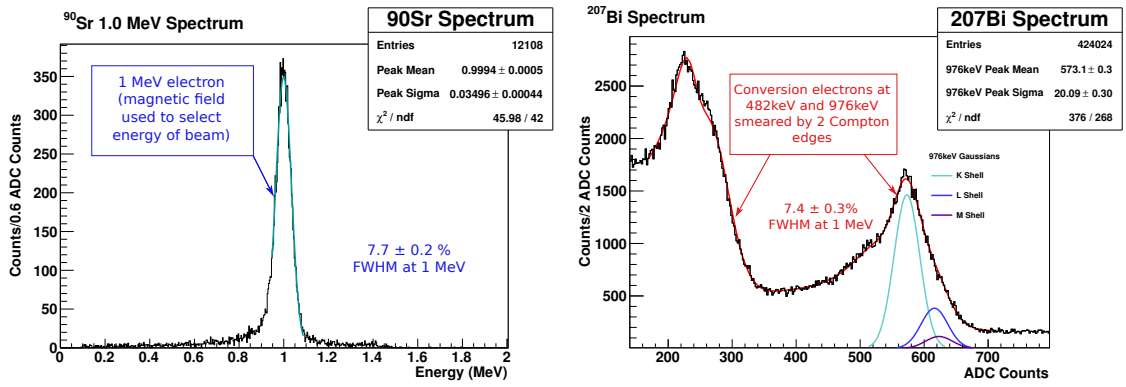


(a) $^{90}$Sr method (b) $^{207}$Bi method

Figure 4: Two different fitting procedures for energy resolution acquisition using (a) $^{90}$Sr and (b) $^{207}$Bi for a 255mm $\varnothing$ $\times$180mm hexagonal EJ-200 block coupled to an 8" Hamamatsu R5912-MOD PMT via Glycerol coupling fluid, with 75$\mu$m PTFE wrapping on the sides and 12$\mu$m Mylar wrapping on the entrance face. The two methods are consistent with each other, with a $\Delta$E/E of 7.7$\pm$0.2% FWHM at 1MeV measured with $^{90}$Sr and of 7.4$\pm$0.3% FWHM at 1MeV measured with $^{207}$Bi. Systematic corrections have been taken into account for both of the results, introduced by the respective data acquisition systems.

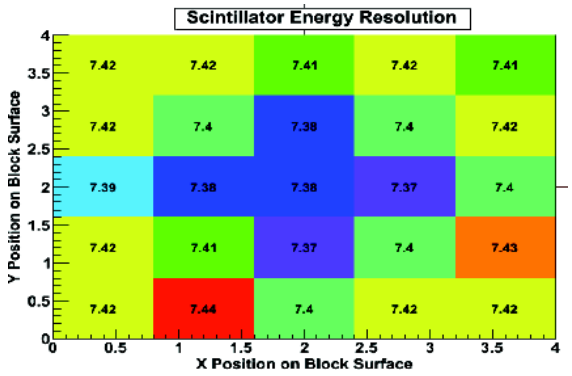


Figure 5: $\Delta$E/E FWHM at 1MeV comparison for $256^2$mm$^2$ and $308^2$mm$^2$ PST and PVT scintillator blocks.

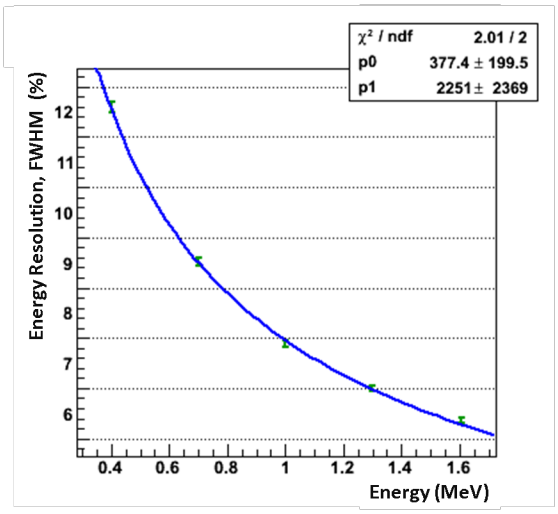


Figure 6: Energy resolution as a function of $^{90}$Sr energy using a $256^2$mm$^2$ ENVINET square block and a Hamamatsu R5912-MOD PMT.

the beam energy, which follows a $\sqrt{E}$ distribution (Figure 6).

The time resolution of the system is measured by an LED signal delivered to two optical modules in coincidence.

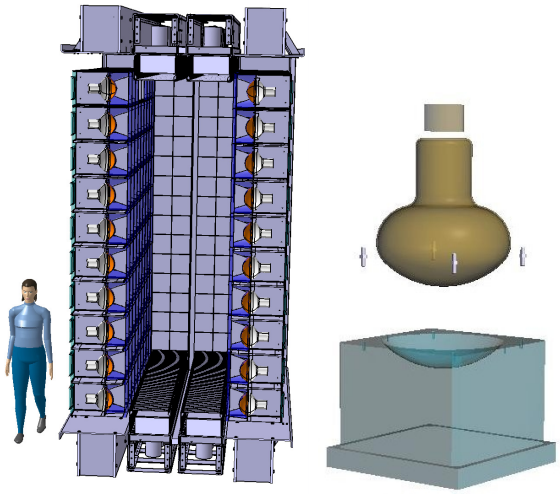

(a) The SuperNEMO calorimeter

(b) SuperNEMO optical module

Figure 7: The SuperNEMO calorimeter (a) and a blown up SuperNEMO calorimeter optical module: a $256^2$mm$^2$ block coupled to an 8" PMT (b).

## 5. Calorimeter Design

The SuperNEMO calorimeter (Figure 7(a)) consists of a polyvinyl-toluene (PVT) or polystyrene (PST) plastic $256^2$mm$^2$ square scintillator block with a minimal thickness of 120mm and a hemispherical 'cutout' directly coupled to an 8" PMT (Figure 7(b)) covered by a magnetic shield. The block is wrapped in 0.024g/cm$^2$ Teflon on the sides and 12$\mu$m aluminised Mylar on the entrance face to increase the light collection. Many different configurations have been tested to reach this configuration. The first SuperNEMO module, known as the 'demonstrator', calorimeter will consist of these $256^2$mm$^2$ block optical modules. The R&D that has led to this design will now be described.

### *5.1. Scintillators*

#### *5.1.1. Material*

It is adequate to use a scintillating detector to reach this target as the $\Delta$E/E that can be achieved is limited by other properties of the detector, such as the thickness of the source foil (which contributes $\sim$ 5% to the detector $\Delta$E/E). The SuperNEMO calorimeter requires a scintillator that has a high light yield, low electron back scattering (which is proportional to Z$^2$), high radiopurity, good timing (requiring a coincidence time resolution of 400ps $\sigma$ of two electrons at 1MeV) and a relatively low cost. A fast inorganic option of YSO ($Y_2SiO_5$ doped with Ce) and Phoswich (a hybrid consisting of two $CaF_2$ scintillators doped with Eu optically coupled to each other) scintillators were considered but did not meet the requirements of radiopurity, back scattering and cost.The most obvious type of scintillator that is able to satisfy all of these requirements simultaneously is organic scintillator. Initially, liquid (toluene based, consisting of 0.5% PPO (2,5-Diphenyloxazole) scintillating agent and 0.0025% of wavelength shifting POPOP (1.4-bis(5-phenyloxazol-2-yl) benzene)) and liquid-plastic hybrid scintillators were considered for the calorimeter. However, due to the difficulty of the mechanical design and the energy loss of electrons in the entrance window of the liquid scintillator container the energy resolution of these types of scintillators was too poor to be considered for the final design.

The two main choices of low Z scintillator are PST, as used by NEMO3, and PVT. The candidate scintillators studied for SuperNEMO are listed in Table 1, with three main manufacturers considered - ENVINET for PST, and Bicron (BC) and ELJEN (EJ) for PVT. JINR Dubna and ISM Kharkiv, both manufacturers of PST, were also considered and tested during the early stages of the R&D. PVT has a higher light yield and longer light attenuation length than PST and is therefore preferable, however there are some concerns with PVT. There can be mechanical difficulties with using PVT such as 'crazing' of the scintillator when it comes into contact with various common substances, requiring great care when casting and handling the scintillator. PVT is more brittle than PST

| Material | $\frac{\Delta E}{E}$(%) |
|---|---|
| NEMO-3 PST | 8.9 ±0.2% |
| EJ-200 PVT | 8.3 ±0.2% |
| EJ-204 PVT | 7.8 ±0.2% |

Table 2: Tests of PVT and PST materials, using a scintillator of a $308^2$mm$^2$ square and 124mm depth geometry and a Photonis 8" XP1866 PMT.

and hence more difficult to machine. The cost of PVT is also higher than PST, therefore it was important to consider both PVT and PST for the R&D. A comparison of measurements made with PVT and PST materials is shown in Table 2, confirming that PVT gives a better ΔE/E.

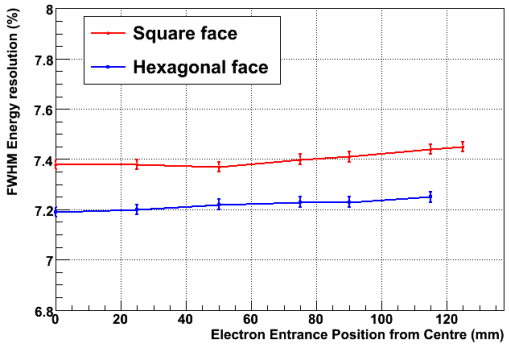


Figure 8: Simulation comparison of hexagonal and square PVT blocks (with the area of the front face normalised to 65946.2mm$^2$) showing energy resolution as a function of position of the entry of 1MeV electrons relative to the centre of the blocks.

*5.1.2. Geometry and Optical Coupling*

The geometry of the scintillator is optimised for the requirements described in Section 2, considering the number and size of optical modules needed for the calorimeter. Several geometries have been closely studied, including hexagonal (255mm and 276mm diameter) and square ($256^2$mm$^2$ and $308^2$mm$^2$) blocks. MC simulations and measurements were carried out to optimise the shape of the scintillator, leading to a choice of a hexagonal (280mm$^{hex}$) or square ($256^2$mm$^2$) face scintillator with a minimum thickness of 120mm. Simulations and measurements (Figure 8) have shown that normalising the area of the particle entrance face of a square block to the same as that of a hexagonal give similar ΔE/E results, with the square block chosen for the final design due to easier manufacturing and construction.

There is a minimum 20mm high 'step' of 10mm width surrounding the particle entrance face of the block. This is required to fully absorb the electrons incident on it (20mm is required for electrons up to 3MeV from the baseline $^{82}$Se and 31mm for 4MeV from $^{48}$Ca). Over this distance the block edges must be straight in order to avoid any loss in detection efficiency (Figure 9). Due to the presence of a ∼ 25 Gauss magnetic field in SuperNEMO the PMT of the optical module needs to be protected with a magnetic shield, covering 10cm of the scintillator in front of the PMT entrance face (Figure 15). In order to achieve a good packing fraction for the optical modules the $\mu$-metal shield rests on the 6mm wide and 20mm high step of the scintillator block. Therefore a step of minimum 20mm and a height of 100mm on top of that is required for the scintillator block, leading to 150mm (Figure 9).

Comparisons of optical modules with and without lightguides were made. Removing the lightguide from the setup reduces the number of optical contacts in the module, a high number of which could lead to poorer light collection. The hemispherical 8" PMT is instead directly coupled to the scintillator, which has a hemispherical cutout of a 112mm radius. This is one of the largest effects on and achieved a significant improvement for ΔE/E (Figure 16). The final geometry of the scintillator block is shown in Figure 9.

Good optical coupling between the scintillator and PMT is essential for uniform and complete light collection, mostly achieved by coupling the PMT directly to the scintillator, as described above. However, it was also im-

| Material | Type | Light Yield (ph/1MeV $e^-$) | Refr. Index | Decay Time (ns) | Atten. Length (cm) | $\lambda$ (nm) |
|---|---|---|---|---|---|---|
| PST | ENVINET | $\sim 8,000$ | 1.57 | 2.5 | 200 | 420-440 |
| PST | JINR Dubna | $\sim 8,000$ | 1.57 | 2.5 | 200 | 420-440 |
| PST | ISM Kharkiv | $\sim 8,000$ | 1.57 | 2.5 | 200 | 420-440 |
| PVT | BC-404 | 10,400 | 1.58 | 1.8 | 160 | 408 |
| PVT | BC-408 | 10,000 | 1.58 | 2.1 | 380 | 425 |
| PVT | BC-412 | 9,200 | 1.58 | 3.3 | 400 | 434 |
| PVT | EJ-204 | 10,400 | 1.58 | 1.8 | 160 | 408 |
| PVT | EJ-200 | 10,000 | 1.58 | 2.1 | 380 | 425 |
| PVT | EJ-212 | 9,200 | 1.58 | 2.4 | 400 | 423 |

Table 1: SuperNEMO calorimeter candidate scintillators and their characteristics, where $\lambda$ is the wavelength of maximum emission (nm). The refractive index is quoted at a wavelength of 589.3nm.

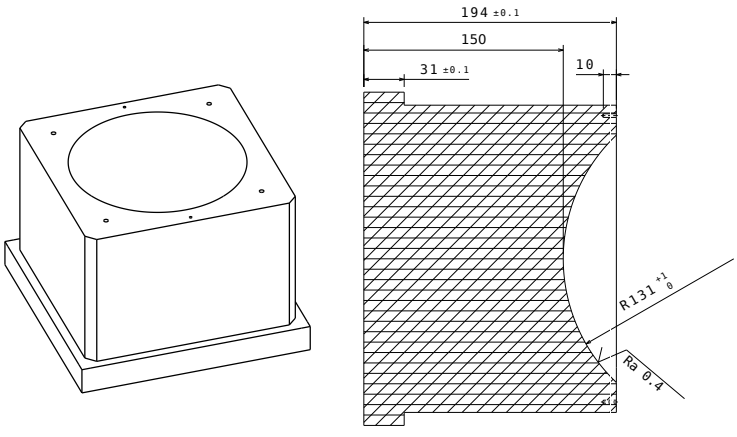


Figure 9: Geometry of the $256^2$mm$^2$ scintillator block.

| Optical Material | Refractive Index | $\frac{\Delta E}{E}(\%)$ |
|---|---|---|
| Alcohol | 1.37 | 9.4 ±0.2% |
| Gel | 1.46 | 8.6 ±0.2% |
| Gel | 1.52 | 8.4 ±0.2% |
| RTV 615 | 1.41 | 9.4 ±0.2% |

Table 3: Tests of optical coupling materials, using EJ-200 PVT for a scintillator of a $308^2$mm$^2$ square and 124mm depth geometry and a Hamamatsu R5912-MOD PMT.

portant to test the coupling material used between the PMT and scintillator, which has to have a refractive index in between the scintillator (1.58) and the PMT glass (1.47) ones, good transmittance, good radiopurity, the correct viscosity and must be non permanent in order for the PMTs to be replaceable. Tests have been carried out on optical gels with different optical indices, showing a large improvement for a gel with a refractive index of 1.52 (Table 3).

An optical epoxy silicone rubber compound (RTV 615 based, with a refractive index of 1.41) is currently to be used to couple the PMTs to the blocks in the construction of SuperNEMO. The compound has a lower refractive index than needed, but has high radiopurity and the required viscosity and is therefore used as a compromise of the requirements. However, work is ongoing to find an optimal coupling material with a closer matching refractive index and other required properties.

#### *5.1.3. Wrapping and Surface Finishing*

In order to increase light collection, the optical modules must be wrapped in a reflective material, which must have high reflectivity (to redirect any escaped light back to the PMT) and be radiopure. In addition, the reflective material on the scintillator entrance face must have a low Z and low density (to reduce electron back scattering) and must be dimensionally thin (to prevent energy loss of electrons as they pass through the material). The reflectors studied include aluminised Mylar, PTFE (Teflon ribbon or ELJEN EJ510 reflective paint) and Enhanced Specular Reflector (ESR). ESR is a relatively new polymer based product, which is composed of layers that form a gradient of refractive indices. It works by refracting light with an incident angle $\theta_i < \theta_c$ (where $\theta_c$ is the critical angle) to the next layer until $\theta_i > \theta_c$ and has a high reflectance of $\sim 95\%$. Energy resolution can depend on whether specular or diffusive reflectors are used (Table 4).

Optical simulations and measurements have shown that the best $\Delta$E/E is achieved with three layers of diffusive Teflon wrapping (corresponding to an optimal thickness of $0.024$g/cm$^2$) on the sides of the blocks and with $12\mu$m of aluminised Mylar on the sides and the entrance face of the scintillator, which has to be thin enough to avoid electron energy loss inside it but thick enough to shield the optical module from the UV photons produced in the SuperNEMO tracker.

Studies have been carried out to see what kind of surface finishing would get the best performance from the optical module, leading to all surfaces of the scintillator being of a machine finish, except for the face with the hemispherical cutout, which will be polished.

### *5.2. PMTs*

The SuperNEMO calorimeter requires a PMT with a high QE, good collection efficiency and high radiopurity at a reasonable cost. Different size PMTs were considered for SuperNEMO, starting with a 5" PMT (anything smaller would not be viable due to the large number of channels and cost) and going up to an 11" PMT. During testing it was found that using a 5" PMT did not achieve the required $\Delta$E/E as its size did not match the geometry and size of the chosen scintillator blocks. 10" and 11" PMTs did not achieve

| PMT Type | Scintillator | | Reflector | | $\frac{\Delta E}{E}$(%) |
|---|---|---|---|---|---|
| | Type | Dim. (mm) | Side | Face | |
| 8" Ham. | EJ-200 | $255^{hex}\varnothing\times100$ | ESR | Al-Mylar | 7.6 ±0.3% |
| 8" Ham. | EJ-200 | $255^{hex}\varnothing\times100$ | PTFE | Al-Mylar | 7.4 ±0.3% |
| 8" Phot. | ENVINET PST | $255^{hex}\varnothing\times100$ | PTFE | Al-Mylar | 10.7 ±0.2% |
| 8" Phot. | ENVINET PST | $255^{hex}\varnothing\times100$ | Al-Mylar | Al-Mylar | 11.0 ±0.2% |

Table 4: Tests of specular and diffusive reflective materials, where the 8" Hamamatsu is the R5192-MOD tube and the 8" Photonis is the XP1886-124 tube.

the required ΔE/E due to an insufficient collection efficiency from the photocathode to the first dynode, which becomes smaller for larger diameter PMT bulbs. This led to a choice of an 8" PMT, which increases the photo-detection surface to improve the ΔE/E and decreases the total number of calorimeter channels used (and hence improves radiopurity and reduces cost). 8" and larger diameter PMTs have so far been mostly used for Cerenkov light detection, offering a large surface and high gain ($10^8$ - $10^{10}$) to detect the few photo-electron ($N_{pe}$) output. In SuperNEMO the level of light is $\sim$ 1000 $N_{pe}$, therefore the PMTs have had to undergo development to focus the linearity to take into account any non linear effects due to the high light level. The QE, collection efficiency, gain (considering voltage dividers and the number of dynode stages) and shape of the PMTs have also been studied.

Most of the R&D tasks described could only be carried out in partnership with PMT manufacturer companies, prompting the SuperNEMO collaboration to start close work with Photonis and Hamamatsu in 2005. ET Enterprises PMTs were also considered and tested, however did not have the QE required for SuperNEMO. Photonis and Hamamatsu started the development of 8" PMTs (XP1886 from Photonis and R5912-MOD from Hamamatsu, Table 5), with the main focus on increasing the QE of the photocathode, the reduction on the number of dynode stages from 11 to 8, decreasing the gain by a factor of 100 and the geometry of the dynodes (with a linear focused geometry to give good linearity and minimise the transit time of electrons for a fast response).

*5.2.1. Photocathode*

The development of new photocathode processes in recent years has been achieved with bi-alkali alloys, such as SbKCs and SbKNa [5], leading to a peak QE of $\sim$ 40% for 3" PMTs. These photocathodes have a spectral sensitivity optimal in the U.V. - blue region, thus are a good match for the $\lambda$ emission of the SuperNEMO scintillators (Table 1). Photonis and Hamamatsu have worked on extrapolating these processes to 8" PMTs and have produced several tubes with QE at or above $\sim$ 40% at $\sim$400nm (Figure 10). For comparison, the average QE of the 1940 3" and 5" PMTs used in NEMO3 was 20%.

As the QE of a PMT is wavelength ($\lambda$) dependent it is important to match the $\lambda$ of the scintillator light output as closely as possible to that of the peak $\lambda$ of the PMT. Therefore the development of the scintillators and the PMTs must be correlated with respect to each other.

Several prototypes of 8" PMTs have been received and tested by the collaboration. Although the QE of the Hamamatsu tubes is higher, the Photonis tubes were found to give a better ΔE/E. In 2009 Photonis announced a full stop to their PMT R&D branch, therefore there has been a strong focus on improving the ΔE/E for the Hamamatsu PMTs. A lower collection efficiency in the Hamamatsu

| Type | Cathode ⌀ (in) | Quoted Max QE | QE at 400nm | Dynode Stages | Gain at Nominal HV |
|---|---|---|---|---|---|
| Hamamatsu R5912-MOD | 8 | 42% | 41% | 8 | $5 \times 10^5$ at 1500V |
| Photonis XP1886 | 8 | 35% | 35% | 8 | $5 \times 10^5$ at 1500V |
| ET Enterprises 9354KB | 8 | 28% | 26% | 12 | $7 \times 10^6$ at 1300V |

Table 5: The main SuperNEMO calorimeter candidate PMTs and their characteristics for the best selected tubes.

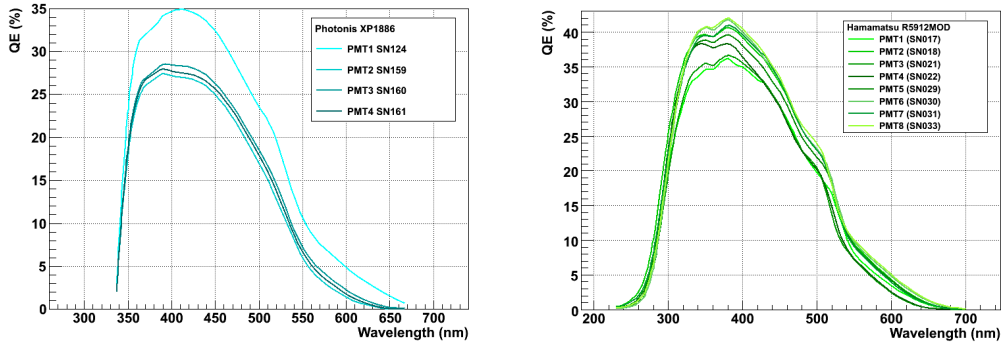


(a) Photonis QE

(b) Hamamatsu QE

Figure 10: Quantum efficiency curves of bi-alkali photocathodes for several 8" PMTs from (a) Photonis (XP1886) and (b) Hamamatsu (R5912-MOD) measured by the respective manufacturers after production.

tubes compared to the Photonis tubes was suspected and after addressing that aspect of the tube development, the difference between the performance of the tubes decreased but was still present. After investigating it was found that this was due to a problem with the spatial uniformity of the photocathode in the Hamamatsu tubes. Measurements have shown that the QE is constant over almost the entire surface of the Photonis PMTs (Figure 11(a)), but decreases by up to 30% for photons incoming on the side of the PMT compared to the centre for the Hamamatsu tubes (Figure 11(b)). After further development with Hamamatsu the photocathode uniformity was improved to being constant across almost the entire surface of the PMT (Figure 11(c), improving the $\Delta$E/E obtained with the Hamamatsu PMTs (Table 6).

SuperNEMO is a low counting rate experiment, therefore the polarity of the PMTs was chosen to be positive. This minimises the noise due to field emissions and lowers the dark currents of the PMTs.

*5.2.2. Gain and Linearity*

The average SuperNEMO light level is $\sim$ 1000 $N_{pe}$ (for 1 MeV electrons), corresponding to an instantaneous peak current of $\sim$ few mA, which makes keeping linearity challenging. Several details have been considered and implemented in the design of the 8" PMTs to ensure a linear response: 8 dynode stages, a focused linear geometry of the dynodes and an increasing electric field on the last dynode stages. Ten of the Hamamatsu 8" PMTs have been received and tested after being coupled to plastic scintillators. Measurements carried out with the $^{90}$Sr electron spectrometer in the energy range of 0.4 - 2 MeV (Figure 12) and with an LED in the energy range of 0 - 5 MeV (Figure 13) show that the deviation from linearity does not exceed 0.5% (Figure 12). Therefore we can expect to have linearity better than 2% up to 3MeV.

Decreasing the number of dynode stages and optimising the voltage divider also decreases the gain on the PMT. The distribution of high voltage (HV) between dynodes is obtained with a voltage divider circuit. Typically, a linear distribution of tensions gives a homogeneous acceleration of electrons between all of the dynodes to maximise the gain. In order to decrease the gain, the distribution at the last dynode stages was changed to a progressively increasing one (Figure 14), giving an electric field that increases at the end of the signal amplification and hence preventing non-linearity of the response.

*5.2.3. Collection Efficiency*

The HV distribution of the first two stages of the voltage divider was also optimised to improve the collection efficiency of the photoelectrons and hence the $\Delta$E/E. This was achieved by increasing the HV between the cathode and the first dynode (by 2) and between the first and second dynodes (by 1.5) and achieved an improvement of $\sim$ 0.4% for absolute $\Delta$E/E (Table 7). The Hamamatsu PMTs currently still have a poorer collection efficiency than Photonis, however the required $\Delta$E/E has now been obtained with both due to Hamamatsu's higher QE (Table 8).

Studies have been carried out in collaboration with Phynics Cie and Photonis to characterise the minimum length of the magnetic shield over the photocathode required to shield the PMT from the magnetic field in order not to see any effect on the collection efficiency of the PMT. This length was found to be 10cm (Figure 15).

*5.2.4. Timing*

Reducing the number of dynode stages of the PMT helped to reduce the time transition spread (TTS) of the PMT, improving the timing of the calorimeter. The hemispherical shape of the PMT also ensures better timing.

The main focus of the calorimeter development has been on optimising the light collection for $\Delta$E/E, therefore the time resolution

| Block number | PMT | $\frac{\Delta E}{E}$ (%) | Gain (nVs) | Rise Time (ns) |
|---|---|---|---|---|
| 1 | R5912-MOD BI | 8.0 ± 0.1 | 4.9 ± 0.1 | 4.1 ± 0.3 |
| | R5912-MOD AI | 7.5 ± 0.1 | 5.4 ± 0.1 | 4.4 ± 0.3 |
| 2 | R5912-MOD BI | 7.7 ± 0.1 | 4.8 ± 0.1 | 4.3 ± 0.3 |
| | R5912-MOD AI | 7.3 ± 0.1 | 5.8 ± 0.1 | 4.3 ± 0.3 |

Table 6: Tests of Hamamatsu R5912-MOD PMTs before and after photocathode uniformity improvements, using two $256^2$mm$^2$ EJ-204 square scintillator blocks wrapped in 0.024g/cm$^2$ of Teflon on the sides and 12$\mu$m on the entrance face and coupled to the PMTs via alcohol, where BI indicates the PMT before improvement and AI indicates the PMT after improvement, run at the nominal HV.

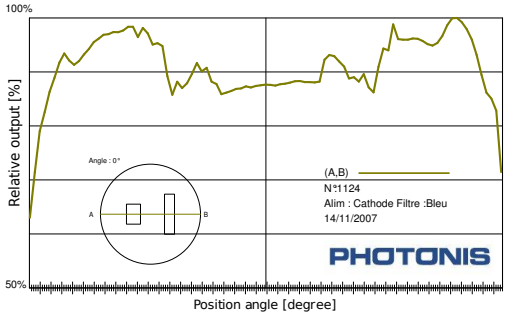


(a) Photonis uniformity [6]

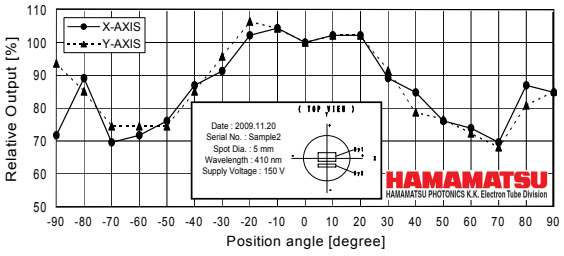


(b) Hamamatsu uniformity (before improvement)

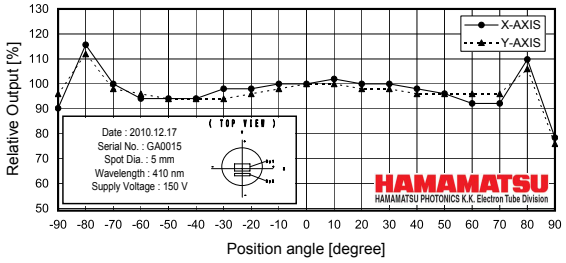


(c) Hamamatsu uniformity (after improvement)

Figure 11: Photocathode uniformity response of (a) Photonis, (b) Hamamatsu PMTs before improvement and (c) Hamamatsu PMTs after improvement, measured in relative units with three prototypes of PMTs.

| Configuration | K-Dy1 | Dy1-Dy2 | $\frac{\Delta E}{E}$ (%) |
|---|---|---|---|
| Standard | | | 8.5 ±0.2% |
| Altered | ×2 | ×1.5 | 8.1 ±0.2% |

Table 7: Tests of an optimised HV divider using an EJ-204 PVT scintillator of a $308^2$mm$^2$ square geometry and a Hamamatsu R5912-MOD PMT, where K denotes the cathode and Dy1 and Dy2 denote the first and second dynodes respectively.

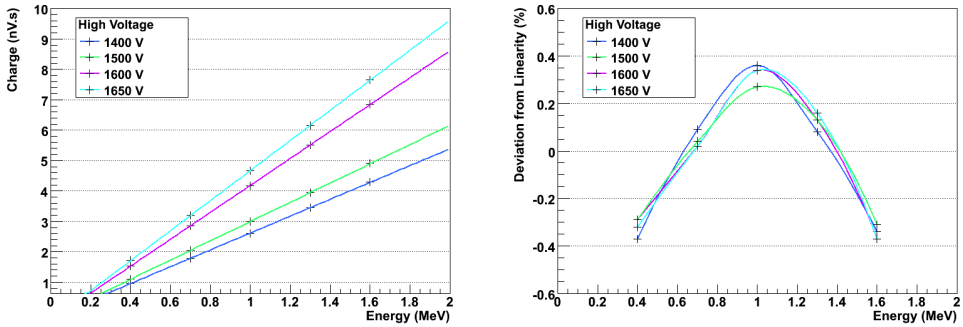


(a) Charge response (b) Deviation from linearity

Figure 12: Charge response of a SuperNEMO scintillation counter with a new 8" PMT (R5912-MOD Hamamatsu) as a function of the electron energy (a) and the observed deviation from a linear fit (b) using the electron spectrometer for testing. The energy resolution at 1MeV is 7.9%, corresponding to $\sim$ 885 $N_{pe}$ detected in the PMT.

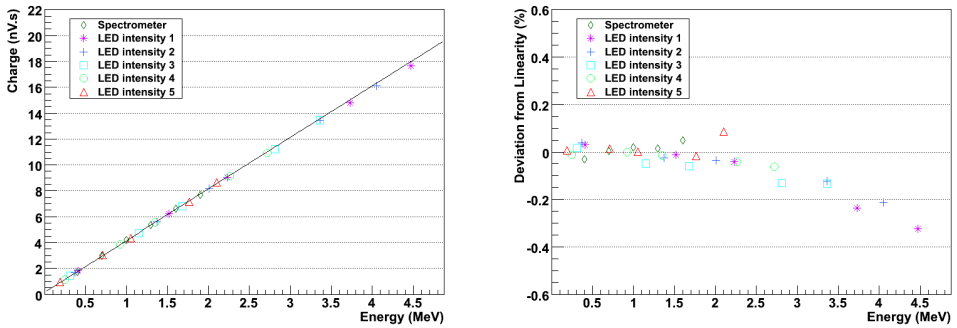


(a) Charge response (b) Deviation from linearity

Figure 13: Charge response of a SuperNEMO scintillation counter with a new 8" PMT (R5912-MOD Hamamatsu) as a function of the electron energy (a) and the observed deviation from a linear fit (b) using an LED for testing.

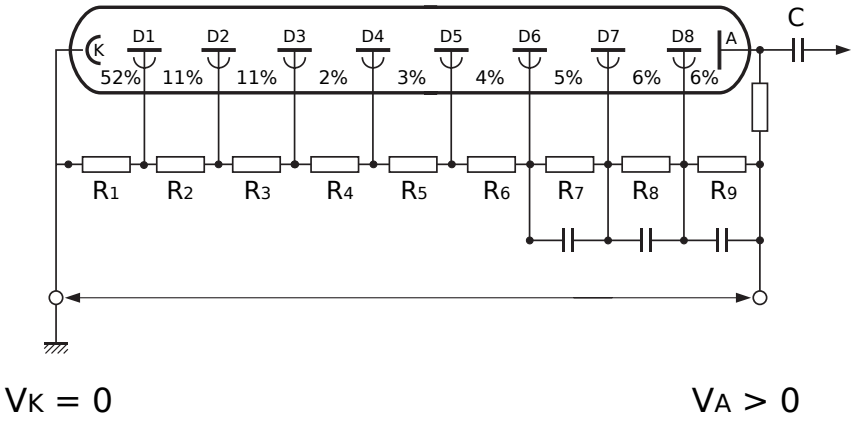


Figure 14: A SuperNEMO PMT 8 dynode stage voltage divider circuit, with the value of the voltages between each stage given in percent.

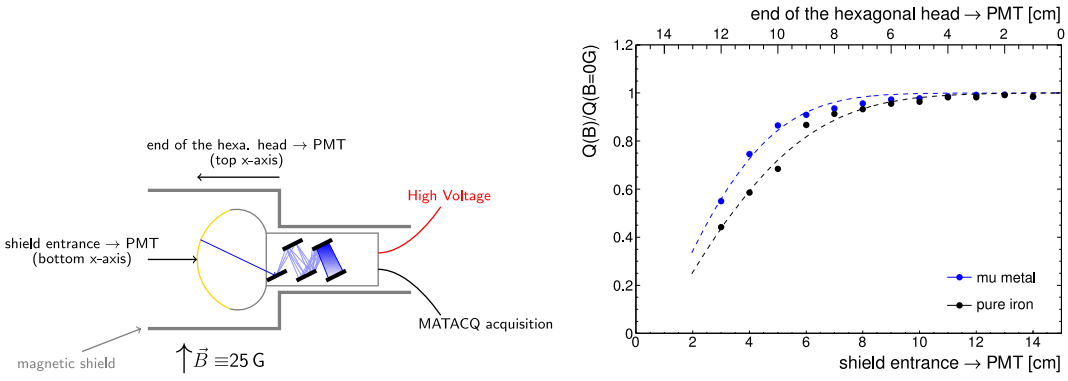


(a) SuperNEMO optical module

(b) Relative collection efficiency

Figure 15: A SuperNEMO optical module (a) and relative collection efficiency (b) as a function of distance to cover PMT photocathode in a 25G magnetic field.

has only been validated for the configurations that have achieved the required ΔE/E.

*5.2.5. Pulse Parameters*

PMT afterpulses could lead to an increased counting rate of the calorimeter by creating false $\gamma$ hits in the SuperNEMO detector. If included in the charge integration of pulses they could also degrade the ΔE/E. PMTs with afterpulses with a delay of up to 2$\mu$s (caused by light ions in the PMT) can be identified and undergo a selection criteria requiring the probability of afterpulses occurring to be $< 1\%$, with $\sim x\%$ of PMTs passing the selection. The dark noise of the PMTs has to be $< 5$Hz for a five photo-electron output.

*5.2.6. Radiopurity*

The glass and internal insulation components of the PMT are the main source of contamination in the calorimeter. The current level of radiopurity reached for the Hamamatsu 8" PMTs is 0.58Bq/kg for $^{40}$K, 0.10Bq/kg for $^{214}$Bi and 0.02Bq/kg for $^{208}$Tl, which is sufficient for the SuperNEMO baseline isotopes. The expected levels to reach are 0.05Bq/kg for $^{214}$Bi and 0.004Bq/kg for $^{208}$Tl. This is compared to 0.53Bq/kg for $^{40}$K, 0.24Bq/kg for $^{214}$Bi and 0.01Bq/kg for $^{208}$Tl for the NEMO3 5" PMTs [1]. The SuperNEMO collaboration is currently working closely with the Primeverre high purity glass manufacturer to produce a low radioactivity PMT bulb necessary for lower $Q_{\beta\beta}$ value isotopes, requiring an order of magnitude radioactivity improvement.

To ensure radiopurity, all of the componets of the optical module, particularly the PMT components and glass, are selected with high purity Germanium (HP-Ge) detectors.

## 6. Summary and Conclusion

The SuperNEMO experiment aims to reach a sensitivity of $10^{26}$ years with 100kg of $^{82}$Se. One of the main focuses of the project R&D has been on the calorimeter design, in particular improving the energy resolution of electrons from 14-17% to 7% FWHM at 1 MeV using larger volume plastic scintillators. Many combinations of PMTs, scintillators, reflective wrappings and their parameters have been tested to arrive at the optimal optical module for the SuperNEMO calorimeter. It consists of a $256^2$mm$^2$ square PVT or PST scintillator block, directly coupled to an 8" Hamamatsu R5912-MOD PMT (developed in collaboration with Hamamatsu) via a hemispherical cutout in the scintillator. The block is wrapped in 0.024g/cm$^2$ Teflon on the sides and 12 $\mu$m al-Mylar on the entrance face of the scintillator to increase light collection. The collaboration has achieved the ΔE/E stipulated by the R&D proposal, with the main results summarised in Table 8. There have been early indications that the ΔE/E of 8.7 ±0.2% for a $256^2$mm$^2$ PST scintillator block with an 8" R5912-MOD Hamamatsu PMT can be further improved. A single block from the latest production has been measured to give a result of 8.0 ±0.2% ΔE/E at 1 MeV.

The contribution of each part of the R&D to the improvement in ΔE/E can be seen in Figure 16, where the starting point is the ΔE/E of NEMO3 ($\frac{14-17\%}{\sqrt{E}(MeV)}$) and the endpoint is the ΔE/E of SuperNEMO ($\frac{7\%}{\sqrt{E}(MeV)}$). The largest improvement for ΔE/E comes from the direct coupling of the 8" PMT to the hemispherical cutout in the scintillator block without the use of a light guide, therefore avoiding any unnecessary loss of light collection. Another large contributing factor to the ΔE/E improvement comes from the increase in quantum efficiency of the bi-alkali photocathodes of the 8" PMTs. Optimising the material, wrapping and surface finishing, and the geometry of the scintillator block and the operation of the PMT (optimisation of the voltage divider, gain and linearity) have also contributed to reaching the target ΔE/E.

Construction of the SuperNEMO 'demon-

| | Scintillator Dimensions | Hamamatsu | Photonis |
|---|---|---|---|
| PST | 256 x 256 x 120 $cm^3$ | 8.7 ±0.2% | 7.5 ±0.2% |
| PVT | 256 x 256 x 120 $cm^3$ | 7.3 ±0.2% | 6.7 ±0.2% |

Table 8: Measurements of the final SuperNEMO optical module designs.

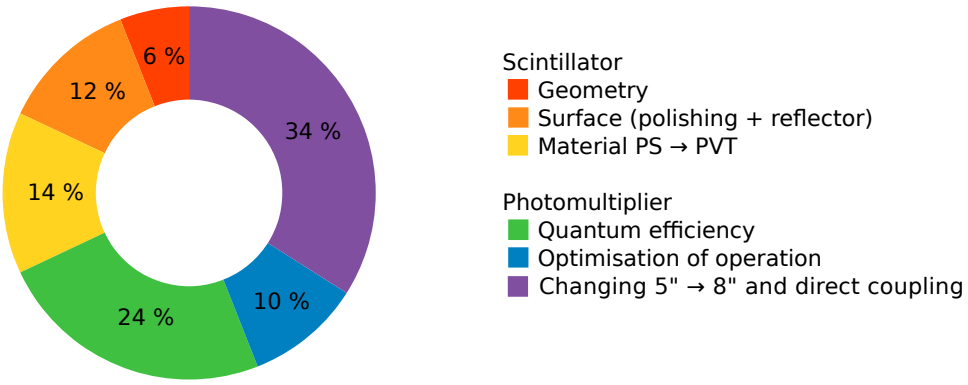


Figure 16: Contribution of performance developments to reach the SuperNEMO optical module design starting at the level of NEMO3.

strator' module is currently under way, which will be a fully operational standalone module containing 7kg of $^{82}$Se. The demonstrator will be installed and commissioned in the Laboratoire Soutterain de Modane (LSM) and begin running in 2015. Depending on the results of the demonstrator, the rest of the detector will start construction in 2015, with each module being commissioned and starting running as soon as it is complete. SuperNEMO aims to reach its sensitivity by 2020.

## References


[1] Arnold R. et al. Technical design and performance of the NEMO3 detector. *Nucl. Instrum. Meth.*, A **536**:79-122, 2005.

[2] Arnold R. et al. Probing new physics models of neutrinoless double beta decay with SuperNEMO. *Eur. Phys. J.*, C **70**:927-943, 2010.

[3] B. Pahlka et al. Spectral modelling of the scintillator for the NEMO-3 and SuperNEMO detectors. *Nucl. Instrum. Meth.*, A **625**:20, 2011.

[4] Ponkratenko O. A. et al. The event generator DECAY4 for simulation of double beta decay processes and decay of radioactive nuclei. *Phys. Atom. Nucl.*, **63**:1282-1287, 2000.

[5] Kapista M. et al. Breakthrough in quantum efficiency of bi-alkali photocathode PMTs, *IEEE*, NSS'07.

[6] Photonis Internal Document UBP-1967-06.